Journal of Engineering Research and Reports

Volume 26, Issue 11, Page 286-303, 2024; Article no.JERR.126740
ISSN: 2582-2926

Dynamic Simulation and Analysis of Three Phase Induction Motor for Faults Detection using Matlab/Simulink

Ekop Ubong Sebastian [a], Ekom Enefiok Okpo [a] and Imo Edwin Nkan [a*]

[a] Department of Electrical and Electronic Engineering, Akwa Ibom State University, Ikot Akpaden, Nigeria.

Authors' contributions

This work was carried out in collaboration among all authors. All authors read and approved the final manuscript.

Article Information

DOI: https://doi.org/10.9734/jerr/2024/v26i111331

Open Peer Review History:
This journal follows the Advanced Open Peer Review policy. Identity of the Reviewers, Editor(s) and additional Reviewers, peer review comments, different versions of the manuscript, comments of the editors, etc are available here: https://www.sdiarticle5.com/review-history/126740

Original Research Article

Received: 10/09/2024
Accepted: 13/11/2024
Published: 19/11/2024

ABSTRACT

The dynamic simulation of three-phase induction motors under fault conditions is essential for understanding and mitigating the impacts of electrical faults on motor performance. This study aims to simulate and analyze the impact of electrical faults on three-phase induction motors to improve fault detection and isolation strategies. Utilizing MATLAB/Simulink software, the behavior of three-phase induction motors under both symmetrical and unsymmetrical faults is modeled and analyzed. The motor's baseline parameters, include 3 Amps rated power and speed of 1500 RPM. Symmetrical faults, such as line-to-line-to-line (L-L-L), and unsymmetrical faults, like single-phase to ground faults, were simulated to observe their effects on motor operation. The d-q model was used to simulate motor dynamics, employing a block model approach to resolve reference frame

**Corresponding author: Email: imonkan@aksu.edu.ng;*

Cite as: *Sebastian, Ekop Ubong, Ekom Enefiok Okpo, and Imo Edwin Nkan. 2024. "Dynamic Simulation and Analysis of Three Phase Induction Motor for Faults Detection Using Matlab/Simulink". Journal of Engineering Research and Reports 26 (11):286-303. https://doi.org/10.9734/jerr/2024/v26i111331.*

theory issues. Major parameters analyzed include rotor speed, electromagnetic torque, and stator current. Through detailed simulations, key performance indicators such as torque fluctuations, current spikes, and decreases in rotor speed are examined. At 1.5 seconds, when the fault was introduced, the rotor speed, electromagnetic torque, and stator current were all affected. For instance, during a symmetrical fault, the rotor speed dropped from 1500 RPM to 1200 RPM, electromagnetic torque declined to -12 Nm, and the stator current increased to 7 Amps from the rated 3 Amps. Under an unsymmetrical single-phase-to-ground fault at the same instant, rotor speed decreased from 1500 RPM to 1400 RPM, electromagnetic torque declined to -12 Nm with greater distortion, and the stator current in the affected phases rose to 7 Amps from the rated 3 Amps. These results underscore the importance of robust fault detection and isolation mechanisms to enhance motor reliability and longevity. This work significantly contributes to engineering by offering validated simulation models and insights into parameter sensitivity, serving as both an educational resource and a foundation for advanced fault detection system development. The findings are applicable in academic research and industrial contexts, providing guidance for improving motor design and fault management strategies.

Keywords: Induction motors; symmetrical fault; unsymmetrical fault; d-q modelling; simulation; MATLAB/Simulink.

1. INTRODUCTION

AC induction motors are among the most commonly used machines in automation. Their primary advantages include simplicity, robust construction, affordability, low maintenance, and compatibility with AC power sources. Various types of AC induction motors are available on the market, each serving different purposes (Rajput et al. 2020 and Innocent et al. 2021). AC induction motors are generally easier to construct compared to DC motors. However, controlling speed and torque in different types of AC induction motors requires a thorough understanding of their configuration and characteristics. On the other hand, DC motors excel in starting and speed control, offering high torque (Ahmed et al. 2020). DC machines operate quietly and have a wide speed range, with minimal electromagnetic interference and high tolerance for overcurrent or inrush current. However, the friction between the commutator and brushes (Iegorov et al. 2020) leads to sparking and mechanical wear, limiting the operational lifespan of DC motors and increasing maintenance costs. This raises concerns about reliability and safety, restricting the use of DC motors in some modern industrial applications, as noted by Wang et al. (2020 and Abunike et al. 2021).

Over the years, motors have transformed the mining and automation industries. Operations such as hoisting and conveyor belt systems, used to transport minerals like gold, coal, and diamonds from both underground and open-pit mines, rely heavily on induction motors (Rahaman et al. 2014). To ensure the reliable functioning of these motors, proper protection systems must be in place to guarantee safe operation under various load conditions. Malfunctions in induction motors can arise from electrical faults, environmental influences, or mechanical failures. Rotor bearings, for instance, may experience overheating or wear due to mechanical stress (Kozjaruk et al. 2018, Nkan & Okpo 2016). Excessive current can also lead to elevated temperatures. Modeling an induction motor is complex due to its non-linear characteristics, which are affected by electromagnetic saturation and the considerable temperature variations within the synchronous motor setup (Maleki et al. 2020).

In a synchronous motor, the rotor turns at the same speed as the stator's magnetic field, whereas in an induction motor, the rotor rotates at a slightly lower speed than the stator field. This difference causes the magnetic field in the induction motor's stator to rotate relative to the rotor, generating an opposing current in the rotor, which essentially acts as the motor's secondary winding (Izanlo et al. 2020 and Chiba et al. 2022). The rotating magnetic flux induces currents in the rotor windings (Awah et al. 2022) much like how currents are induced in the secondary winding of a transformer. These induced currents create magnetic fields in the rotor that interact with the stator's magnetic field. According to Lenz's Law, the rotor's magnetic field opposes the change in current through the rotor windings. The rotating magnetic field in the stator is responsible for the induced current in the rotor windings, so to counteract this current

change, the rotor spins in the direction of the stator's magnetic field. The rotor continues to accelerate until the induced rotor current and torque equalize with the load. Since no rotor current is induced when rotating at synchronous speed, an induction motor always runs slightly below this speed. The difference, known as "slip," between the actual and synchronous speeds typically ranges from 0.5% to 5.0% for standard Design B induction motors (Jara et al. 2016).

The key characteristic of an induction motor is that torque is generated solely by induction, unlike synchronous or DC motors where the rotor is externally excited, or permanent magnet motors where the rotor is self-magnetized (Izanlo, et al. 2020 and MG 2011). For currents to be induced in the rotor, its speed must be lower than the stator's rotating magnetic field (ns); otherwise, there would be no relative motion between the magnetic field and the rotor conductors, and no current would be induced. As the rotor slows down below synchronous speed, the relative movement of the magnetic field within the rotor increases, inducing more current in the windings and producing greater torque. The ratio between the speed of the induced magnetic field in the rotor and the stator's rotating magnetic field is referred to as "slip." Under load conditions, the rotor speed decreases, causing the slip to increase enough to generate the torque required to drive the load. For this reason, induction motors are often called "asynchronous motors" (Innocent et al. 2021 and Cavagnino, et al. 2022).

Induction motors can also function as induction generators or can be modified to form linear induction motors, which produce direct linear motion. However, operating an induction motor in generator mode is more complex due to the need to excite the rotor, which relies on residual magnetization at startup. In some instances, this residual magnetization is sufficient for self-excitation under load. To achieve excitation, the motor may need to be briefly connected to a live grid or paired with capacitors initially charged by the residual magnetism, which then supply the reactive power during operation. Similarly, when operating in parallel with a synchronous motor acting as a power factor compensator, the induction motor behaves in a comparable way. In generator mode, when connected to the grid, the rotor speed is higher than in the motoring mode, enabling the transfer of active power to the grid (Babbage et al. 1825, Izanlo et al. 2020). One drawback of the induction motor as a generator is its high consumption of magnetizing current. Most researchers rely on simplified models to analyze the performance of induction motors.

In studies conducted by Babbage et al. (1825), (Izanlo et al. 2020, Chitra et al. 2006). the authors presented a simulation of an induction machine using a fuzzy logic approach. This method was employed to regulate the speed of the induction machine, aiming to achieve optimal torque with minimal losses. The field-oriented control technique was applied to develop a fuzzy logic controller that significantly enhanced motor torque control, even under varying performance conditions. The design was tested using various MATLAB toolboxes, and the results demonstrated an improvement in the induction motor's efficiency under stable operating conditions. Their findings indicated that the proposed speed regulator was both effective and reliable.

In another study, (Heber et al. 1997) introduced the use of a genetic algorithm (GA) to analyze experimental loads on an induction machine. The GA-based method was used to predict motor parameters from experimental data, with typical no-load and blocked rotor tests serving as the basis for parameter identification. The study focused on optimizing the cost equation, which involved minimizing the stator currents and rotor speed, while also examining the effect of differential equations on parameter estimation. The estimated speed and torque parameters derived from the mathematical model were compared with experimental results, showing a strong correlation that validated both the equation and the GA technique for improving motor performance.

Similarly, (Elnaghi et al. 2019) applied the genetic algorithm to obtain parameters that linked the proposed method to the motor’s loading process through an evaluation function. The GA was tested on three different simulated load scenarios, with results showing a notable reduction in overall motor losses. This approach proved effective for parameter estimation and motor performance optimization.

The research described in (Sadasivan & Omana 2011) involved the simulation of an induction motor using both an artificial neural network (ANN) and an adaptive neuro-fuzzy inference system (ANFIS) to analyze variables that are typically difficult to measure. These methods

were applied to test 20 induction motors with different power ratings. The experimental results included measurements of starting torque, current, maximum torque, full-load slip, efficiency, rated active power, and reactive power. The authors compared the results obtained from the ANN and ANFIS models with practical data and observed a strong correlation between the predicted and actual values. However, the ANFIS model proved to be more accurate than the ANN model.

In the studies conducted by (Jirdehi & Abbas 2016) a step-by-step Simulink implementation of an induction motor was developed using the stator and rotor equations in the stator reference frame. The research highlighted the effective use of reference frame theory as a powerful method for analyzing the performance of induction machines. The relevant equations were first introduced, followed by the development and implementation of a generalized model of a three-phase induction motor in a clear, step-by-step process. The primary aim of the research was to simulate the induction motor model in MATLAB/Simulink and examine the effects of speed, torque, and stator and rotor currents on the motor's performance characteristics. In conclusion, a dynamic model of a three-phase induction motor was successfully implemented and simulated in MATLAB/Simulink, yielding satisfactory results in terms of torque and speed characteristics. Future work is planned to include the simulation of the induction motor model, considering the effects of flux saturation and supply-side harmonics.

The study of Torque vs. Speed characteristics of an induction motor through mathematical modeling using SIMULINK was conducted in (Chen et al. 2010, Asif et al. 2016). It was noted that over the past three decades, the application of induction motors has significantly increased due to their high efficiency and improved speed control. In (Batool et al. 2013) a MATLAB/Simulink implementation of an induction motor was presented using reference frame theory to simulate a five-phase induction motor. A dynamic model was utilized to gain a deeper understanding of the motor's behavior in both steady-state and transient conditions.

Several of the works reviewed above focused on the dynamic modeling and simulation of three-phase induction motors but did not address fault detection. Additionally, the use of MATLAB/Simulink in these studies was not thoroughly explored for fault analysis. This research will focus on the dynamic modeling of a three-phase induction motor, specifically in relation to potential faults, and MATLAB/Simulink software will be employed for this investigation.

2. METHODOLOGY

This project begins with a comprehensive review of existing literature focused on the dynamic simulation of three-phase induction motors and their behavior under fault conditions. This step provides foundational knowledge on how motors react to faults, explores various fault detection techniques, and identifies potential areas for improvement. The insights gained inform both the mathematical modeling of the motor and the simulation approach, ensuring alignment with current research standards and best practices. After the literature review, mathematical expressions are formulated to precisely size and define the motor parameters essential for modeling fault behavior as shown in Fig. 1. This includes the development of key equations such as stator flux equations which represent the flux linkages within the stator windings, influencing current flow and torque generation. Rotor flux equations which are essential for analyzing induced electromotive forces and understanding rotor behavior during faults. Stator and rotor current equations which allow for a detailed examination of how currents vary during faults, particularly with sudden spikes or drops. Electromagnetic torque equation which quantifies the torque produced by the motor, providing insight into how torque changes when faults occur. Mechanical system equation which described the motor’s rotational dynamics, this equation models how the motor’s speed and torque respond to changes in load and fault conditions. Once the mathematical model is developed, the project then re-evaluates available simulation tools to determine the most suitable platform. MATLAB/Simulink is selected for its comprehensive suite of tools for dynamic system modeling and its library of electrical component blocks. Its advantages include, detailed simulations of induction motor dynamics under both normal and fault conditions, with accuracy in behavior replication. Compatibility with other toolboxes to enables simulations across multiple domains, facilitating control design, signal processing, and parameter optimization. MATLAB/Simulink’s environment also allows engineers to incorporate advanced functionalities and expand the model for various experimental needs. With the equations

established, they are implemented in Simulink using appropriate blocks from the Simulink library. Each aspect of the motor's dynamics flux, current, torque, and mechanical systems is modeled using Simulink blocks. For example, flux and current equations were implemented using integrators and gain blocks to replicate the mathematical functions accurately. Torque and mechanical dynamics were modeled using dynamic system blocks to represent motor movement and torque response under load and fault conditions. After constructing the Simulink model, the motor's behavior is simulated under various scenarios, including normal operation and different fault types (e.g., symmetrical and unsymmetrical faults). The output waveforms, such as rotor speed, stator current, and electromagnetic torque, are studied to assess the motor's response. Key performance indicators like current spikes, torque fluctuations, and rotor speed changes are analyzed in detail, giving insights into the motor's fault response. Based on the initial simulation results, further refinements are made to enhance model accuracy. Adjustments to parameters, block configurations, or additional components ensure the model more accurately reflects real-world motor behavior. This iterative process allows for continuous improvement and optimization of the model, enhancing the fault detection capabilities of the motor.

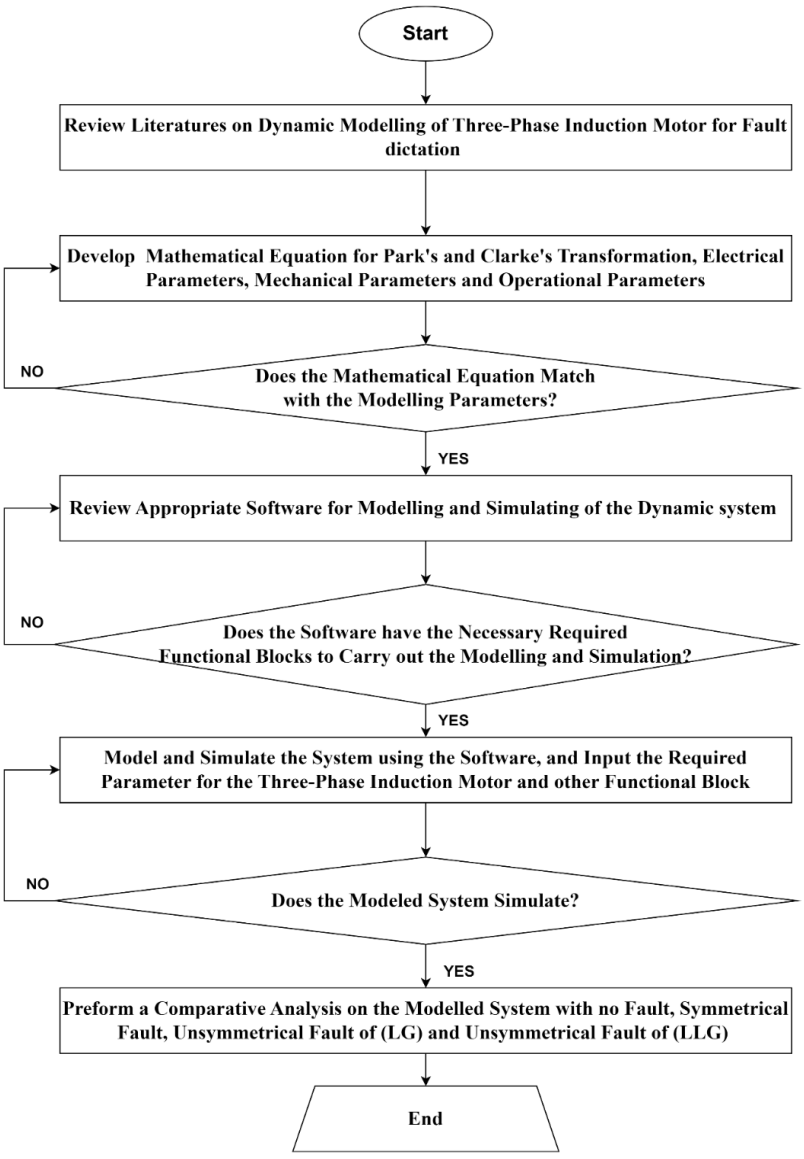

Fig. 1. Flow chart of the research paper

3. DYNAMIC MODELLING OF THREE PHASE INDUCTION MOTOR

All analysis and simulation in this paper are based on the d-q or dynamic equivalent circuit of the induction motor represented in the rotating reference frame (Aher & Thosar, 2016, Krause et al. 1995) shown in Fig. 2. The differential equations produced from analysis of the circuits in Fig. 2 are as follows:

$$v_{ds} = R_s i_{ds} \frac{d\lambda_{ds}}{dt} - \omega_e \lambda_{qs} \quad (1)$$

$$v_{qs} = R_s i_{qs} \frac{d\lambda_{qs}}{dt} - \omega_e \lambda_{ds} \quad (2)$$

$$v_{dr} = 0 = R_r i_{dr} \frac{d\lambda_{dr}}{dt} - (\omega_e - \omega_r)\lambda_{qr} \quad (3)$$

$$v_{qr} = 0 = R_r i_{qr} \frac{d\lambda_{qr}}{dt} - (\omega_e - \omega_r)\lambda_{dr} \quad (4)$$

where d is the direct axis, q is the quadrature axis, $v_{ds}$is the d-axis stator voltage, v_{qs} is the q – axis stator voltage, v_{dr} is d – axis rotor voltage, v_{qr} is q-axis rotor voltage, i_{ds} is the d-axis stator current, i_{qs} is the q-axis stator current, i_{dr} is d-axis rotor current, i_{qr} is q-axis rotor current, R_s is the stator resistance, R_r is the rotor resistance, ω_e is the angular velocity of the reference frame, ω_r is the angular velocity of the rotor, and λ_{qs}, λ_{ds}, λ_{qr}, and λ_{dr} are flux linkages. It is assumed that the induction motor analyzed is a squirrel cage machine, leading to the rotor voltage in (3) and (4) being zero. The flux linkages in (1-4) can be written as:

$$\lambda_{ds} = L_s i_{ds} + L_m i_{dr} \quad (5)$$

$$\lambda_{qs} = L_s i_{qs} + L_m i_{qr} \quad (6)$$

$$\lambda_{dr} = L_r i_{dr} + L_m i_{ds} \quad (7)$$

and

$$\lambda_{qr} = L_r i_{qr} + L_m i_{qs} \quad (8)$$

Where L_r is the rotor self-inductance, L_s is the stator self-inductance, L_m is the magnetizing inductance, L_{Ir} is the rotor leakage inductance, and L_{Is} is the stator leakage inductance. The self-inductances in (5-8) can be expressed as:

$$L_s = L_m + L_{Is} \quad (9)$$

and

$$L_r = L_m + L_{Ir} \quad (10)$$

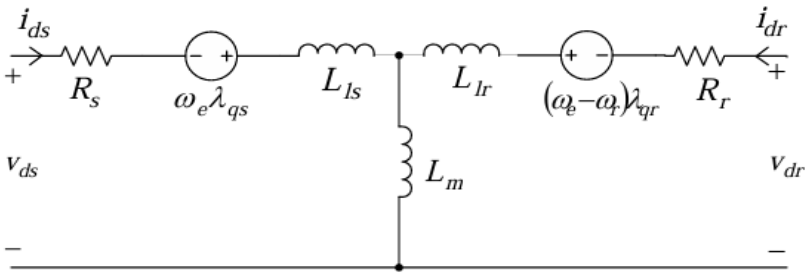

d-axis equivalent circuit

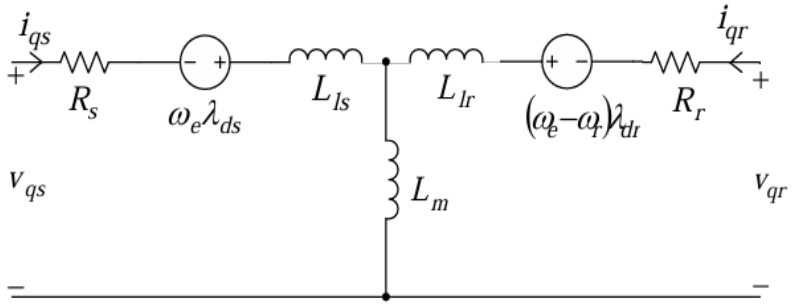

q-axis equivalent circuit

Fig. 2. d-q equivalent circuit of the induction motor (Aher & Thosar 2016)

The currents equations can be written as:

$$i_{ds} = \frac{\lambda_{ds} - L_m i_{qr}}{L_s} \quad (11)$$

$$i_{qs} = \frac{\lambda_{qs} - L_m i_{qr}}{L_s} \quad (12)$$

$$i_{dr} = \frac{\lambda_{dr} - L_m i_{ds}}{L_r} \quad (13)$$

$$and$$

$$i_{qr} = \frac{\lambda_{qr} - L_m i_{qs}}{L_r} \quad (14)$$

After making substitutions, the currents can be expressed in terms of flux linkages as:

$$i_{ds} = \frac{L_r}{L_r L_s - L_m^2}\lambda_{ds} - \frac{L_m}{L_r L_s - L_m^2}\lambda_{dr} \quad (15)$$

$$i_{qs} = \frac{L_r}{L_r L_s - L_m^2}\lambda_{qs} - \frac{L_m}{L_r L_s - L_m^2}\lambda_{qr} \quad (16)$$

$$i_{dr} = \frac{L_s}{L_r L_s - L_m^2}\lambda_{dr} - \frac{L_m}{L_r L_s - L_m^2}\lambda_{ds} \quad (17)$$

$$and$$

$$i_{qr} = \frac{L_s}{L_r L_s - L_m^2}\lambda_{ds} - \frac{L_m}{L_r L_s - L_m^2}\lambda_{qs} \quad (18)$$

Three-phase voltages can be converted to the two-phase stationary frame using the following relationship:

$$\begin{bmatrix} v_{qs}^s \\ v_{ds}^s \end{bmatrix} = \begin{bmatrix} 1 & 0 & 0 \\ 0 & \frac{-1}{\sqrt{3}} & \frac{1}{\sqrt{3}} \end{bmatrix} \begin{bmatrix} v_{an} \\ v_{bn} \\ v_{cn} \end{bmatrix} \quad (19)$$

where the superscript s in (19) refers to the stationary frame. The voltages can be converted from the two-phase stationary frame to the synchronously rotating frame using the following:

$$v_{qs} = v_{qs}^s cos\theta_e - v_{ds}^s sin\theta_e \quad (20)$$

$$and$$

$$v_{ds} = v_{qs}^s sin\theta_e + v_{ds}^s cos\theta_e \quad (21)$$

The current variables are given as:

$$i_{qs}^s = i_{qs} cos\theta_e + i_{ds}^s sin\theta_e \quad (22)$$

$$i_{ds}^s = i_{qs} sin\theta_e + i_{ds}^s cos\theta_e \quad (23)$$

The current equation will now become:

$$\begin{bmatrix} i_a \\ i_b \\ i_c \end{bmatrix} = \begin{bmatrix} 1 & 0 \\ \frac{-1}{2} & \frac{-\sqrt{3}}{2} \\ \frac{-1}{2} & \frac{\sqrt{3}}{2} \end{bmatrix} \begin{bmatrix} i_{qs}^s \\ i_{ds}^s \end{bmatrix} \quad (24)$$

3.1 Simulation using Matlab/Simulink

The approach used to build the Simulink model is a block type or modular approach. The approach is based on the idea presented in (Lipo 2001, Ozpineci & Leon 2003, Okpo & Nkan 2016). However, the goal of this research work is to present the model in a clear and simplified manner that is geared toward undergraduate electric machines and power electronics students. This paper also examines different types of simulations and analyses with a three-phase fault introduce in the system to see the performance of the system without fault and with fault. To begin the construction of the Simulink model of the induction motor, let consider the following equation:

The stator fluxes equation is given by:

$$\frac{d}{dt}\Psi_{ds} = V_{ds} + \omega_d \Psi_{ds} - R_s i_{ds} \quad (25)$$

$$\frac{d}{dt}\Psi_{qs} = V_{qs} - \omega_q \Psi_{ds} - R_s i_{qs} \quad (26)$$

The rotor fluxes equation is given by:

$$\frac{d}{dt}\Psi_{dr} = V_{dr} + (\omega_d - \omega_r)\Psi_{qr} - R_r i_{dr} \quad (27)$$

$$\frac{d}{dt}\Psi_{qr} = V_{qr} + (\omega_q - \omega_r)\Psi_{dr} - R_r i_{qr} \quad (28)$$

The stator current equation is given by:

$$i_{ds} = \frac{L_r}{L_r L_s - L_m^2}\Psi_{ds} - \frac{L_m}{L_r L_s - L_m^2}\Psi_{dr} \quad (29)$$

$$i_{qs} = \frac{L_r}{L_r L_s - L_m^2}\Psi_{qs} - \frac{L_m}{L_r L_s - L_m^2}\Psi_{qr} \quad (30)$$

The rotor current equation is given by:

$$i_{dr} = \frac{L_s}{L_r L_s - L_m^2}\Psi_{dr} - \frac{L_m}{L_r L_s - L_m^2}\Psi_{ds} \quad (31)$$

$$i_{qr} = \frac{L_s}{L_r L_s - L_m^2}\Psi_{ds} - \frac{L_m}{L_r L_s - L_m^2}\Psi_{qs} \quad (32)$$

Where,

$$L = L_r L_s - L_m^2 \quad (33)$$

The electromagnetic torque equation is given by:

$$T_e = \frac{3}{2}\frac{p}{2} L_m (i_{ds} i_{dr} - i_{ds} i_{qr}) \quad (34)$$

Where P is the number of poles and T_e is the electromagnetic torque.

And the mechanical system equation is given by:

$$\frac{d}{dt}\omega_m = \frac{1}{j}(T_e - T_l - B_{\omega m}) \quad (35)$$

Where;

$$\omega_r = \frac{p}{2}\omega m$$

$$\frac{d}{dt}\omega_r = \frac{p}{2j}(T_e - T_l - B_{\omega r}) \quad (36)$$

The complete dynamic model of the three-phase induction motor implemented in Simulink is shown in Fig. 3. A double click on any of the blocks shown in Fig. 3 within the Simulink workspace will pull up a subsystem within each individual block shown in Fig. 3. The details of the construction of the model that follows will be described as if the reader is looking at the model in Fig. 3., while it is opened in the Simulink workspace. This approach is easier to follow if the interested reader would like to construct the model for individual use. A double click on the stator fluxes block shown in Fig. 3., will pull up the subsystem shown in Fig. 4. The subsystem in Fig. 4., implements equation (25) and (26). A double click on the rotor fluxes block in Fig. 3., will pull up the subsystem shown in Fig. 5. The subsystem in Fig. 5., implements (27) and (28). A double click on the stator current Model block shown in Fig. 2., will pull up the subsystem shown in Fig. 6. The subsystem in Fig. 6., implements (29) and (30). A double click on the rotor current block shown in Fig. 3., will pull up the subsystem shown in Fig. 7. The subsystem in Fig. 7., implements (31) and (32). A double click on the L block in Fig. 6 or 7 will pull up the subsystem shown in Fig. 8. The subsystem in Fig., 8 implements (33). A double click on the EM torque block shown in Fig. 3., will pull up the subsystem shown in Fig. 9. The subsystem in Fig. 9., implements (34). A double click on the mechanical system block shown in Fig. 2., will pull up the subsystem shown in Fig. 10. The subsystem in Fig. 10 implements (35) and (36).

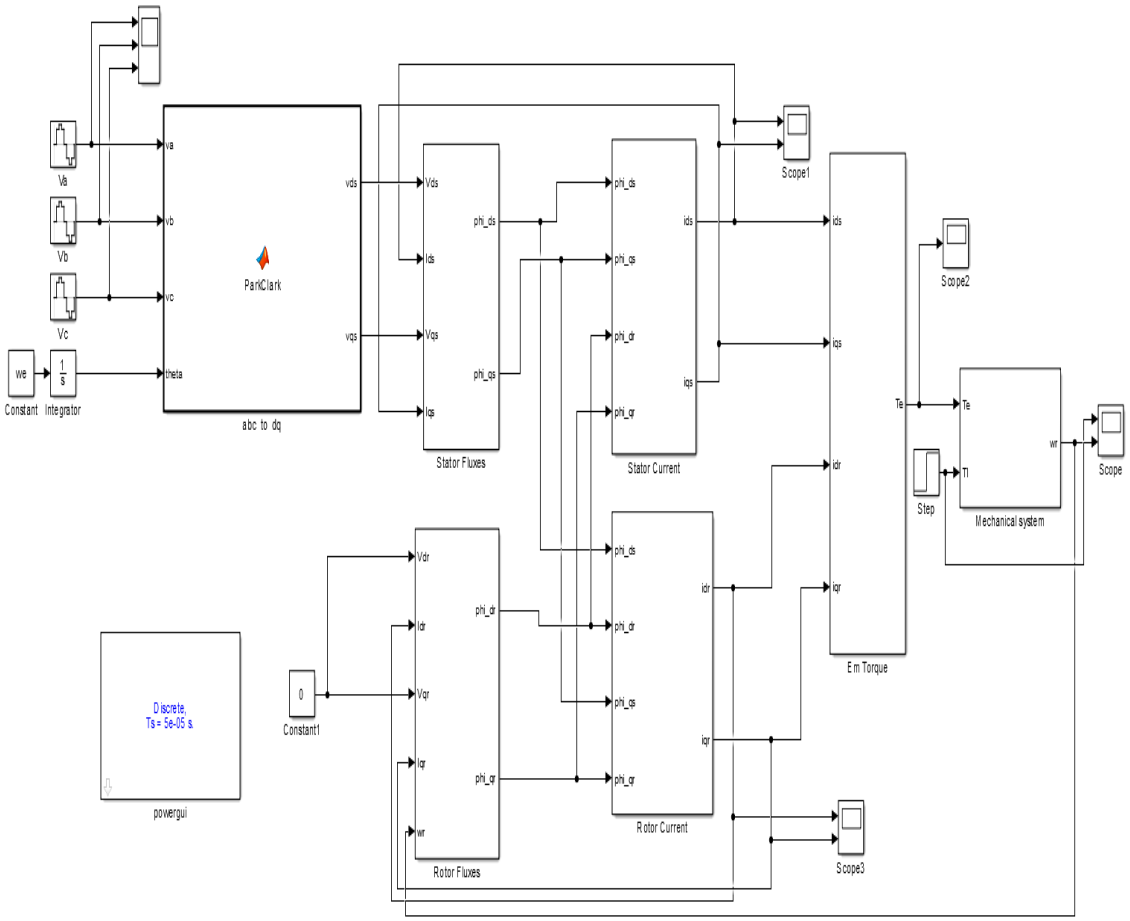

Fig. 3. Complete modelling of the dynamic system with MATLAB/Simulink software

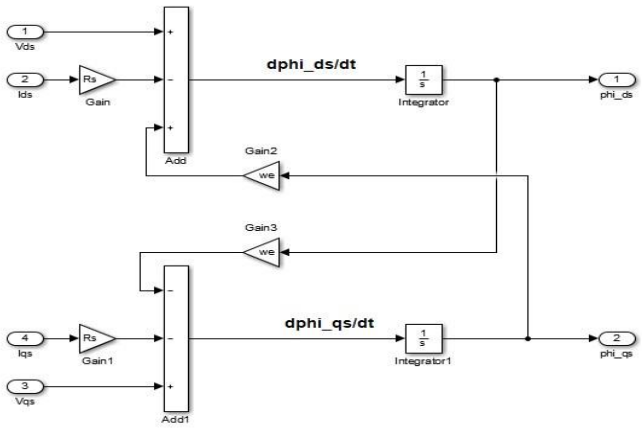

Fig. 4. Subsystem that implements (25) and (26) in Simulink

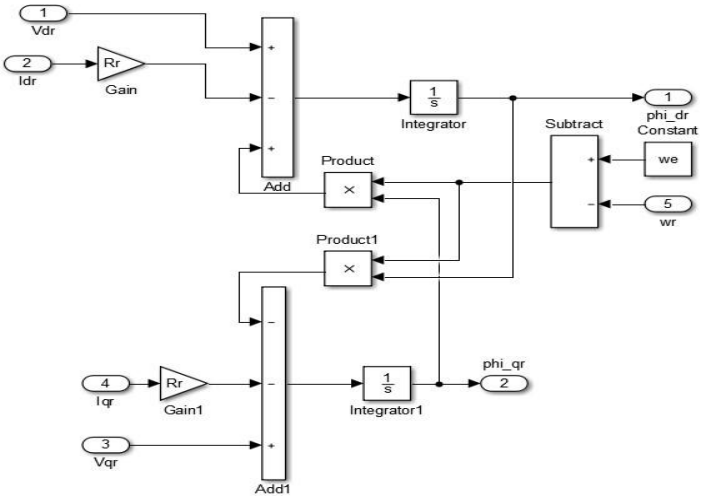

Fig. 5. Subsystem that implements (27) and (28) in Simulink

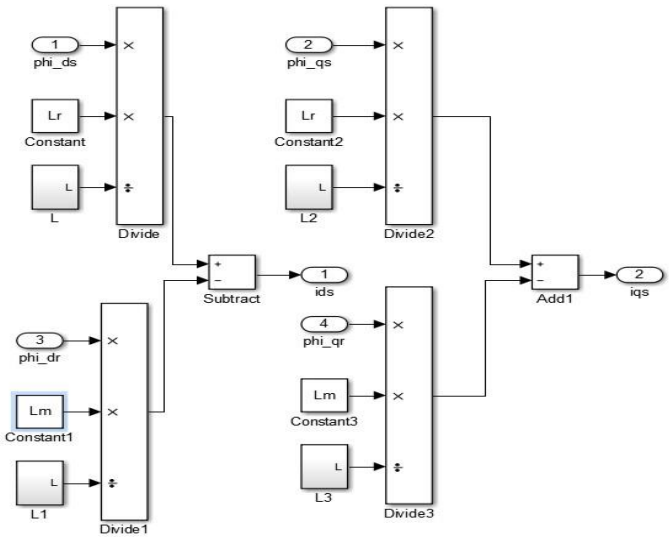

Fig. 6. Subsystem that implements (29) and (30) in Simulink

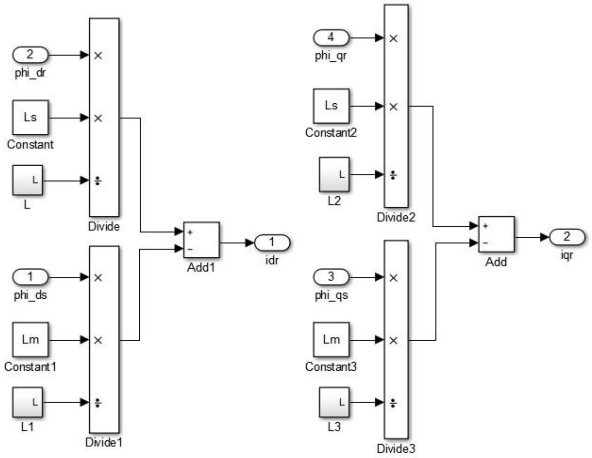

Fig. 7. Subsystem that implements (31) and (32) in Simulink

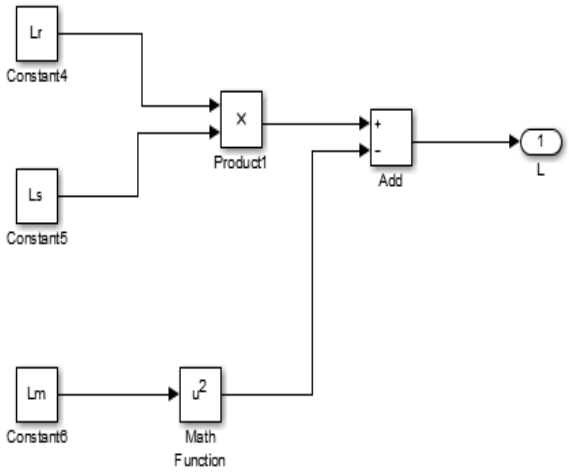

Fig. 8. Subsystem that implements (34) in Simulink.

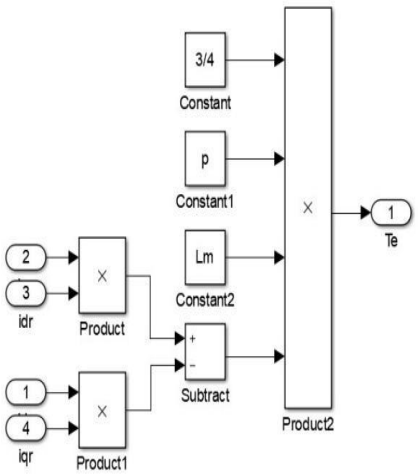

Fig. 9. Subsystem that implements (34)

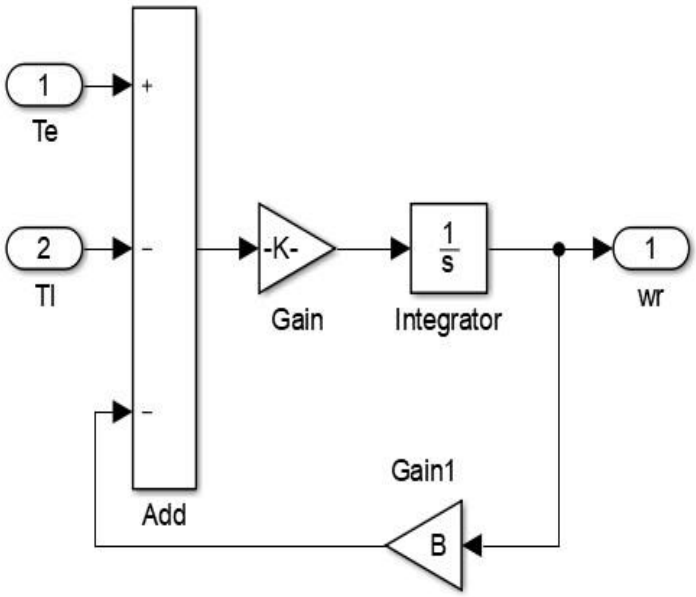

Fig. 10. Subsystem that implements (35) and (36) in Simulink.

The Simulink model shown in Fig. 3., can be simulated in Simulink or from an m file in MATLAB. The m file can be saved, and the Simulink model of the motor can be simulated in MATLAB/Simulink by running the m file.

4. SIMULATION RESULTS AND DISCUSSION

The following parameters were acquired from experimental work with a three-phase induction motor. These settings were then utilized to simulate and examine the behavior of the induction motor without fault and with fault condition. MATLAB/Simulink software was used. The induction motor performance behavior with no fault, symmetrical fault and unsymmetrical fault was presented in term of graphical representation. To analyze the performance behavior of the induction motor without fault, the system was simulated without applying any fault to the voltage supply. The analysis of symmetrical was done by applying a three-phase fault to voltage supply, in this case the voltage magnitude variation across the three phases was reduce from 230 volts to 100 volts simultaneously. The unsymmetrical fault was analyzed with single line to ground fault (LG) and double line to ground fault (LLG). In (LG) fault, the voltage magnitude variation in phase A was reduce from 230 volts to 100 volts, and for (LLG) fault, the voltage magnitude variation in phase A and phase B was reduce from 230 volts to 100 volts respectively.

Table 1. Parameters used for induction motor simulation

Number	Parameters	Value
1	Motor rated power	1.7kW
2	Single phase voltage	230V
3	Stator resistance (R_s)	11.2 Ω
4	Rotor resistance (R_r)	8.3 Ω
5	Stator Inductance (L_s)	0.6255 H
6	Rotor Inductance (L_r)	0.6380 H
7	Magnetizing Inductance (L_m)	0.570 H
8	Total Inertial (j)	0.00214 $kg-m^2$
9	Viscous Friction (B)	0.0041 $Nm-s$
8	Number of poles (P)	4
9	Frequency (f)	50 Hz
10	Slip Speed (w_e)	$2\pi f$

The rated torque was not provided; therefore, before we can calculate the rated torque, the synchronous speed of the machine must first be calculated. The synchronous speed can be calculated as follows:

$$\text{Angular velocity } (\omega) = \frac{2*\pi*N}{60}$$

$$\text{Angular } (\omega) = \frac{2*3.142*1500}{60} = 157\ rad/secs$$

Given the motor output power to be 1700w and ω = 157rad/secs, the full load torque can be calculated as follows;

$$T_l = \frac{1700}{157} = 10.8\ Nm$$

The simulation results are subdivided in the subsequent sections.

4.1. No Fault Analysis

For an induction machine supplied directly by the 250 V three-phase network and running off-no fault, we can visualize the rotor speed, electromagnetic torque and stator current in Fig. 11.

As seen in Fig. 11. a, we have a normal transient state at the rotor speed; the speed start from zero (0) and move to the rated speed which is about 1500 (rpm) and maintain a stable output till 2 seconds without any distortion in the speed. As seen in Fig. 11. b, we have a normal transient state at the electromagnetic torque; however, at start, the electromagnetic torque experiences an increase of 2 to 2.5 the rated torque before it stable at 0.2 seconds and maintain a stable transient state till 2 second. It can be seen in

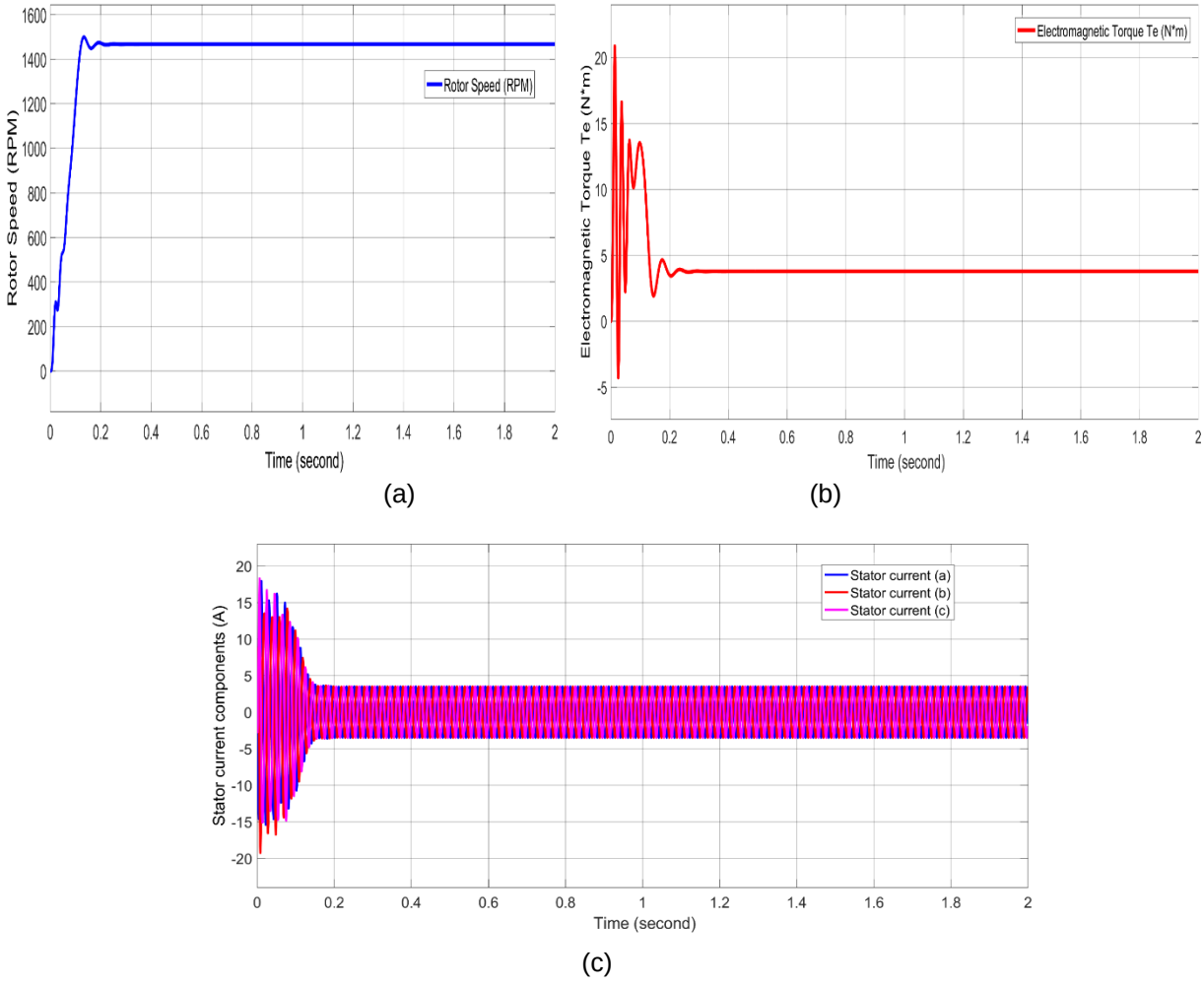

Fig. 11. (a) Rotor speed simulation result at no fault. (b)Electromagnetic torque simulation result at no fault. (c) Stator currents simulation result at no fault

Fig. 11. c, that the stator current also maintain a normal transient state; however, there is a higher current at start, this is as a result of large inrush current at start.

4.2 Symmetrical Fault Analysis

Symmetrical fault in a three-phase induction motor occurs when all three phases experience an equal fault condition. This typically involves either a three-phase short circuit or a three-phase to ground fault, where the fault impedance is the same across all three phases. The analysis of this fault rotor speed, electromagnetic torque and stator current shown in Fig.12.

As seen in Fig. 12. a, we have a normal transient state at the rotor speed from start till 1.5 second when the symmetrical fault occurs; the speed start from zero (0) and move to the rated speed which is about 1500 (rpm) and maintain a stable output till 1.5 seconds when the fault occurs and the speed drop to 1250 (RPM). The speed further drops towards a stall position which if not protected might damage the motor. In Fig. 12. b, we have a normal transient state at the electromagnetic torque; however, at 1.5 second when the fault occurs, the electromagnetic torque experiences a decrease in torque towards a negative axis. It can be seen in Fig. 12. c, that the stator current also maintain a normal transient state; however, there is a sudden increase in stator current at 1.5 seconds, this is as a result of fault that occur.

4.3 Unsymmetrical Fault Analysis (Single Line to Ground)

An unsymmetrical fault in a three-phase induction motor occurs when the fault affects one or two phases unevenly. Fig. 13 shows the fault analysis when single line to ground is affected.

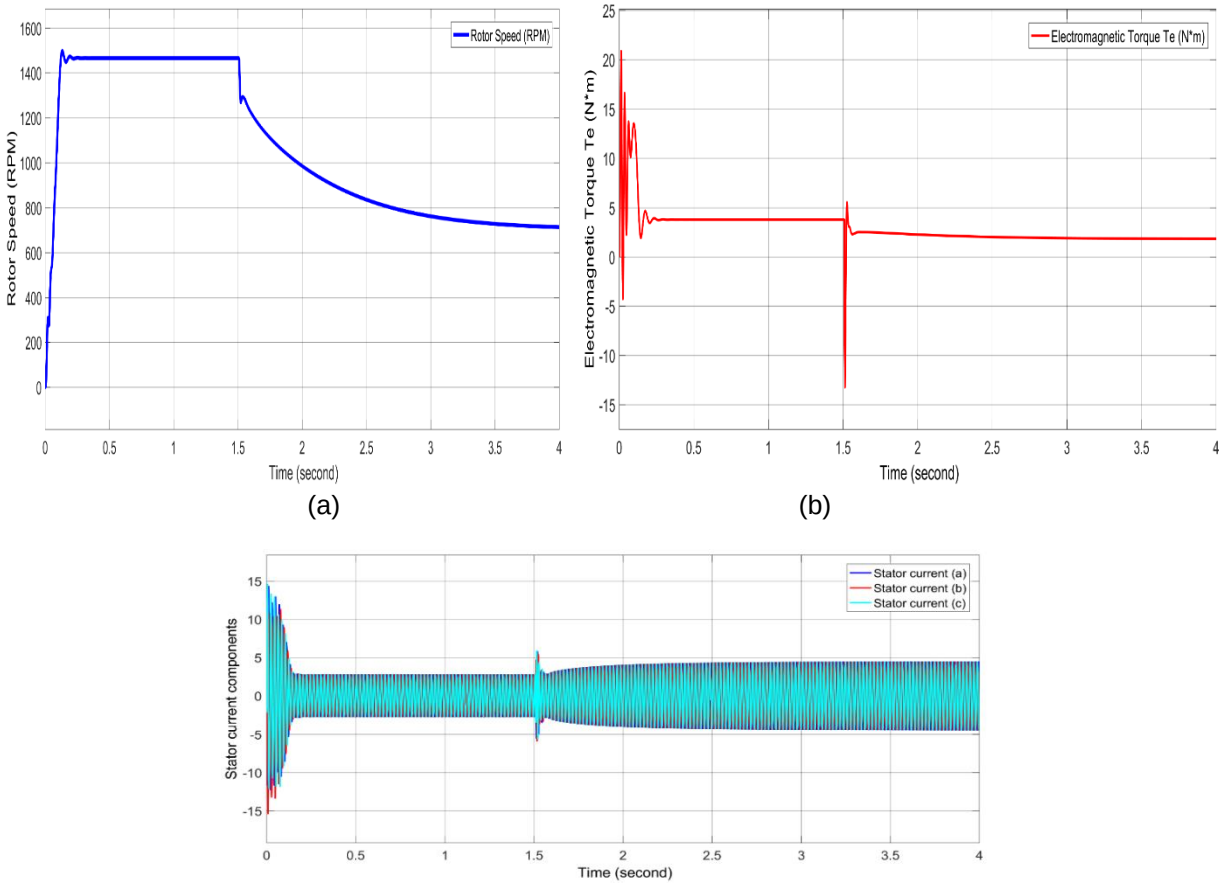

Fig. 12. (a) Rotor speed simulation result at symmetrical fault. (b)Electromagnetic torque simulation result at symmetrical fault. (c) Stator currents simulation result at symmetrical fault.

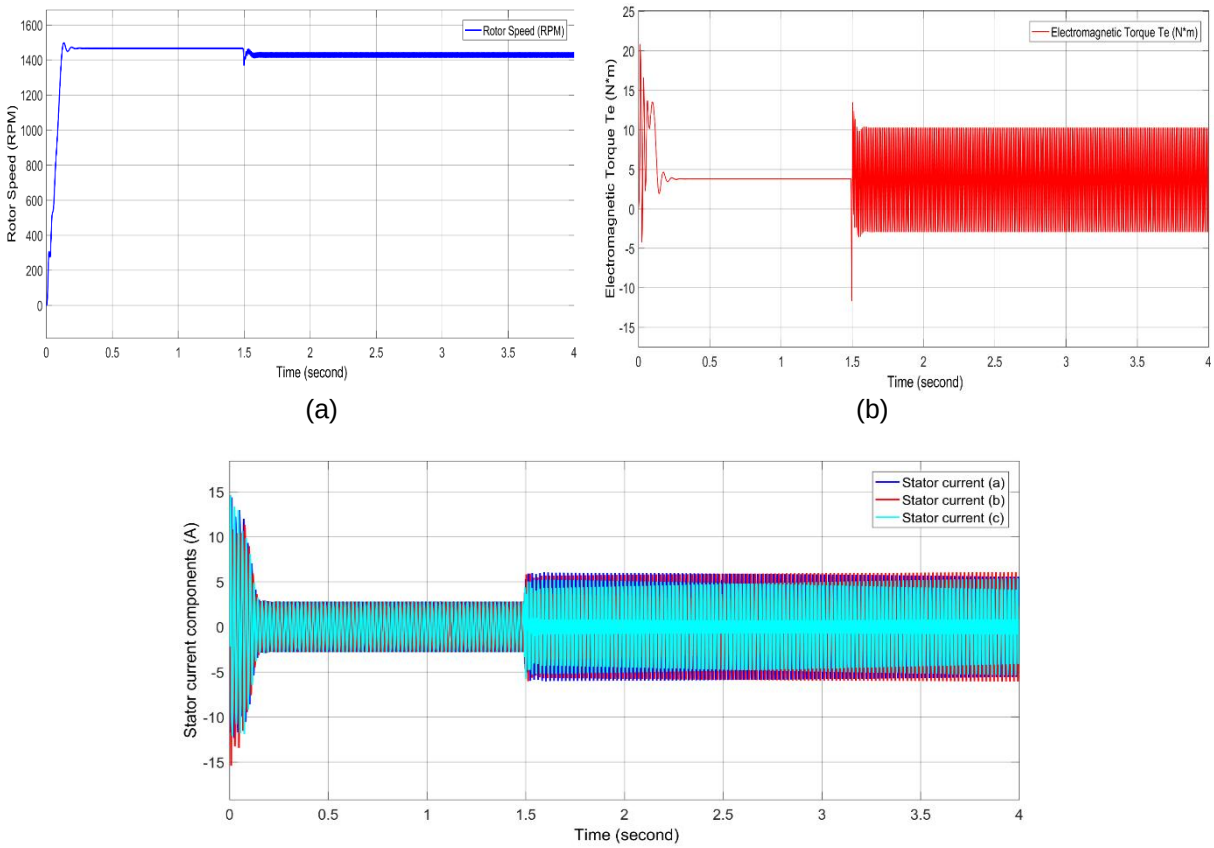

(a) (b)

(c)

Fig. 13. (a) Rotor speed simulation result at unsymmetrical fault (LG). (b)Electromagnetic torque simulation result at symmetrical fault (LG). (c) Stator currents simulation result at symmetrical fault (LG).

As seen in Fig. 13. a, we have a normal transient state at the rotor speed from start till 1.5 second when the unsymmetrical fault of line-to-ground occurs; the speed start from zero (0) and move to the rated speed which is about 1500 (rpm) and maintain a stable output till 1.5 seconds when the fault occurs and the speed drop to 1400 (RPM), and experience a distortion as long as the last. In Fig. 13. b, we have a normal transient state at the electromagnetic torque; however, at 1.5 second when the unsymmetrical fault occurs, the electromagnetic torque experiences a decrease in torque towards a negative axis, and the system could no longer maintain a steady state transient due to the fault. It can be seen in Fig. 13. c, that the stator current also maintain a normal transient state; however, there is a sudden increase in stator current at 1.5 seconds, the increase continues as long as the fault continues, this can be prevented by disconnecting the machine from the supply.

4.4 Unsymmetrical Fault Analysis (Double Line to Ground)

In a double line to ground fault, two of the motor's three phases are short to the ground. During the fault, the induction motor experience torque pulsations, which cause vibration and stress on the rotor and stator. The double line to ground fault analysis is shows in Fig. 14.

As seen in Fig. 14 a, we have a normal transient state at the rotor speed from start till 1.5 second when the unsymmetrical fault of line-to-ground occurs; the speed start from zero (0) and move to the rated speed which is about 1500 (rpm) and maintain a stable output till 1.5 seconds when the fault occurs and the speed drop to 1200 (RPM). It can be notice that, the speed further decreases more than when the machine experience single line-to-ground fault. In Fig. 14 b, we have a normal transient state at the electromagnetic

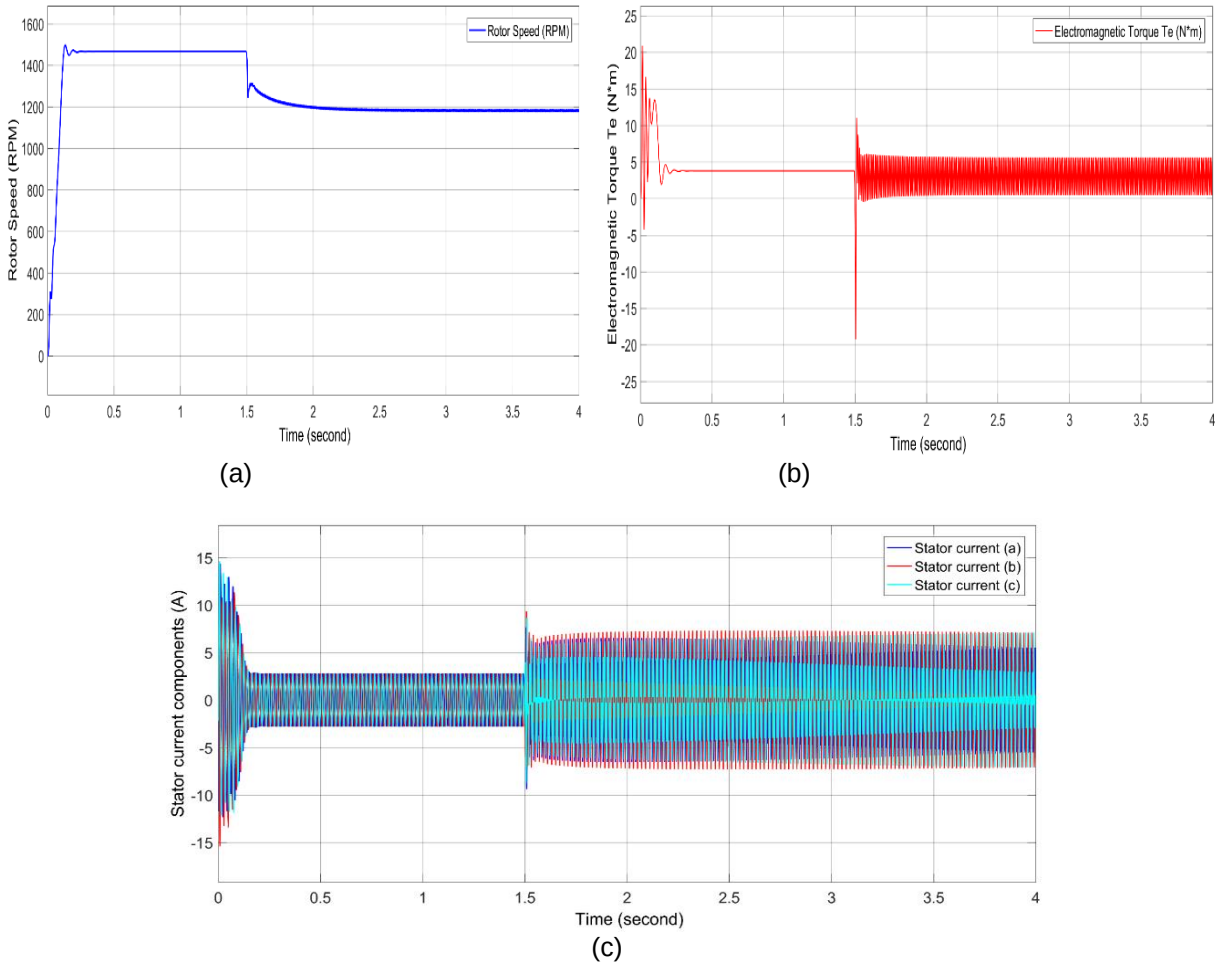

Fig. 14. (a) Rotor speed simulation result at unsymmetrical fault (LLG). (b)Electromagnetic torque simulation result at symmetrical fault (LLG). (c) Stator currents simulation result at symmetrical fault (LLG).

torque; however, at 1.5 second when theunsymmetrical fault occurs, the electromagnetic torque experiences a decrease in torque towards a negative axis. The decrease is much more serve than when the machine experiences a single line-to-ground fault, and the system could no longer maintain a steady state transient due to this fault. It can be seen in Fig. 14 c, that the stator current also maintain a normal transient state; however, there is a sudden increase in stator current at 1.5 seconds, this increase is as a result of the fault that occur in the machine. The stator current in Fig. 14 c is more serve than that of Fig. 13 c, this is because, in Fig. 13 c, one phase is affected but in Fig. 14 c, two phases are affected.

5. CONCLUSION

In this research work, the dynamic simulation of three-phase induction motors under both symmetrical and unsymmetrical fault conditions using MATLAB/Simulink has proven to be an invaluable tool for understanding the complex behaviors of these machines. This project has demonstrated the effectiveness of MATLAB/Simulink in modeling and simulating the intricate dynamics of induction motors, providing detailed insights into their performance under various fault scenarios. Throughout the simulations, it was observed that symmetrical faults, such as line-to-line-to-line fault (L-L-L), lead to significant disruptions in motor operation, causing substantial torque fluctuations and current spikes. These findings align with theoretical expectations and emphasize the importance of robust protection mechanisms in mitigating the adverse effects of such faults. In contrast, unsymmetrical faults, including single-phase to ground faults, presented a different set of challenges. The simulations highlighted the asymmetric current distribution and the resulting

unbalanced magnetic fields, which contribute to increased heating and potential damage to the motor. The detailed analysis of these faults underscored the necessity for precise fault detection and isolation techniques to ensure the reliability and longevity of induction motors. The use of MATLAB/Simulink provided a comprehensive platform for the dynamic simulation, enabling the visualization of motor responses in real-time and offering a flexible environment for testing various fault conditions. The ability to modify parameters and observe outcomes instantaneously facilitated a deeper understanding of motor behavior and enhanced the overall analysis. In summary, this paper has successfully utilized MATLAB/Simulink to simulate and analyze the dynamic responses of three-phase induction motors under both symmetrical and unsymmetrical faults. The insights gained from these simulations are critical for designing effective fault management strategies, improving motor protection systems, and enhancing the overall reliability of induction motor-driven systems. Future work may involve exploring advanced fault detection algorithms and implementing real-time hardware-in-the-loop simulations to further validate and refine the findings from this study.

DISCLAIMER (ARTIFICIAL INTELLIGENCE)

Author(s) hereby declare that NO generative AI technologies such as Large Language Models (ChatGPT, COPILOT, etc) and text-to-image generators have been used during writing or editing of this manuscript.

COMPETING INTERESTS

Authors have declared that no competing interests exist.

REFERENCES

Abunike, E. C., Umoh, G. D., Nkan, I. E., & Okoro, O. I. (2021). Investigating the magnetic characteristics of 12/8 switched reluctance motor for enhanced starting torque. *Nigerian Journal of Technological Development*, 18(1), 70-75.

Aher, S., & Thosar, A. G. (2016). Modeling and simulation of five-phase induction motor using MATLAB/Simulink. *International Journal of Engineering Research and Applications*, 6(5), 1-8.

Ahmed, M., Vahidnia, A., Datta, M., & Meegahapola, L. (2020). An adaptive power oscillation damping controller for a hybrid AC/DC microgrid. *IEEE Access*, 8, 69482-69495.

Asif, M. J., Tayyab, S., Syed, U. H., & Syed, T. H. R. (2016). Mathematical modelling of 3-phase induction motor to study the torque vs. speed characteristics using MATLAB Simulink. In *2016 19th International Multi-Topic Conference (INMIC)*.

Awah, C., Okoro, O. I., Nkan, I. E., & Okpo, E. E. (2022). Impact of structural dimensions and poles on the torque performance of dual-stator permanent magnet machines. *Nigerian Journal of Technological Development*, 19(1), 68-79.

Babbage, C., & John, F. W. H. (1825). Account of the repetition of M. Arago's experiments on the magnetism manifested by various substances during the act of rotation. *Philosophical Transactions of the Royal Society of London*, 115, 467-496.

Batool, M., & Ahmad, A. (2013). Mathematical modeling and speed-torque analysis of three-phase squirrel cage induction motor using MATLAB Simulink for electrical machines laboratory. *International Electrical Engineering Journal (IEEJ)*, 4(1), 880-889.

Cavagnino. (2022). Asynchronous motors. In *Encyclopedia of Electrical and Electronic Power Engineering* (pp. 280-298).

Chen, S., & Živanović, R. (2010). Modelling and simulation of stator and rotor fault conditions in induction machines for testing fault diagnostic techniques. *European Transactions on Electrical Power*, 20(5), 611-629.

Chiba, D., Akamatsu, T., Fukao, T., & Rahman, M. A. (2008). An improved rotor resistance identification method for magnetic field regulation in bearingless induction motor drives. *IEEE Transactions on Industrial Electronics*, 55(2), 852-860.

Chitra, V., & R, S. P. (2006). Induction motor speed control using fuzzy logic controller. *World Academy of Science, Engineering and Technology*, 17-22.

Elnaghi, B. E., Reham, H. M., Sobhy, S., Dessouky, A., & Mariam, K. S. (2019). Load test of induction motors based on PWM technique using genetic algorithm. *International Journal of Engineering and Manufacturing*, 9(1), 1-12.

Heber, B., Xu, L., & Tang, Y. (1997). Fuzzy logic enhanced speed control of an indirect field-oriented induction machine drive. *IEEE Transactions on Power Electronics*, 12(5), 772-778.

Iegorov, O., Olga, I., Oleksandr, M., & Oleksandr, S. (2020). Improving the accuracy of determining the parameters of induction motors in transient starting modes. *Energetika*, 66(1), 1-10.

Innocent, U. O., Nkan, I. E., Okpo, E. E., & Okoro, O. I. (2021). Dynamic response evaluation of a separately excited dc motor. *Nigeria Journal of Engineering*, 28(2), 56-61.

Innocent, U. O., Nkan, I. E., Okpo, E. E., & Okoro, O. I. (2021). Predicting the stability behaviour of three-horse power induction motor using eigenvalue method. *Bayero Journal of Engineering and Technology (BJET)*, 16(2), 66-81.

Izanlo, S. A., Gholamian, S., & Abdollahi, S. E. (2020). Optimal design of a permanent magnet synchronous motor for high efficiency and low cogging torque. *International Journal on Electrical Engineering and Informatics*, 12(2), 173-186.

Izanlo, S., Abdollahi, S. E., & Gholamian, S. A. (2020). A new method for design and optimization of DFIG for wind power applications. *Electric Power Components and Systems*, 48(14-15), 1523-1536.

Jara, W., PiaLindh, J. A., Tapia, I. P., Anna-Kaisa, R., & Juha, P. (2016). Rotor eddy-current losses reduction in an axial flux permanent-magnet machine. *IEEE Transactions on Industrial Electronics*, 63(8), 4729-4737.

Jirdehi, M. A., & Abbas, R. (2016). Parameters estimation of squirrel-cage induction motors using ANN and ANFIS. *Alexandria Engineering Journal*, 55(1), 357-368.

Keerthipala, W. W. L., Duggal, B. R., & Miao, H. C. (1998). Torque and speed control of induction motors using ANN observers. In *1998 International Conference on Power Electronic Drives and Energy Systems for Industrial Growth, 1998. Proceedings* (Vol. 1, pp. 282-288).

Kozjaruk, E., Vasilev, B. U., Shtop, S. A., & Serdukov, N. A. (2018). Currents in bearings of induction motors of electric drives with semiconductor converter. In *Proceedings of the 17th International Ural Conference on AC Electric Drives (ACED)* (pp. 1-5). Ekaterinburg, Russia.

Krause, P. C., Wasynczuk, O., & Sudhoff, S. (1995). *Analysis of electric machinery*. NY: IEEE Press.

Lipo, T. A. (2001). Electric machine analysis and simulation. In *Wiley Encyclopedia of Electrical and Electronics Engineering*.

Maleki, M. G., Chabanloo, R. M., & Farrokhifar, M. (2020). Accurate coordination method based on the dynamic model of overcurrent relay for industrial power networks taking contribution of induction motors into account. *IET Generation, Transmission and Distribution*, 14(4), 645-655.

MG, N. C. (2011). Information guide for general purpose industrial AC small and medium squirrel-cage induction motor standards. *National Electrical Manufacturers Association*.

Nkan, E., & Okpo, E. E. (2016). Electric power forecasting by the year 2020 using the least square method. *International Journal of Research and Advancement in Engineering Science*, 6(1), 205-215.

Okpo, E. E., & Nkan, I. E. (2016). Constructional features and performance analysis of 3-phase linear induction motor. *International Journal of Scientific Innovations and Sustainable Development*, 6(1), 176-185.

Ozpineci, B., & Leon, M. T. (2003). Simulink implementation of induction machine model—a modular approach. In *Proceedings of the IEEE International Electric Machines and Drives Conference, 2003. IEMDC'03*.

Rahaman, N., & G. H. V. (2014). Modeling and simulation of a three-phase electric traction induction motor using MATLAB/Simulink. *International Journal of Electrical, Electronics, and Computer Systems*, 5(2), 1-8.

Rajput, S., Bender, E., & Averbukh, M. (2020). Simplified algorithm for assessment equivalent circuit parameters of induction motors. *IET Electric Power Applications*, 14(3), 426-432.

Sadasivan, P., & Omana, M. (2011). Genetic algorithm based parameter identification of three phase induction motors. *International Journal of Computer Applications*, 10, 51-56.

Sangeetha, M., & Parthiban, B. (2014). Review of modeling and dynamic analysis of three-phase induction motor using MATLAB Simulink. *International Journal of Science, Engineering and Technology Research (IJSETR)*, 3(3), 374-378.

Wang, H., Chau, K. T., Lee, C. H., Cao, L., & Lam, W. H. (2020). Design, analysis, and implementation of wireless shaded-pole induction motors. *IEEE Transactions on Industrial Electronics*, 68(8), 6493-6503.

Peer-review history:
The peer review history for this paper can be accessed here:
https://www.sdiarticle5.com/review-history/126740